S. Yliniemi, S. Honkanen, A. Ianoul, A. Laronche, and J. Albert, Photosensitivity and volume gratings in phosphate glasses for rare-earth-doped ion-exchanged optical waveguide lasers, Journal of the Optical Society of America B 23, 2470-2478 (2006).

Photosensitivity and volume gratings in phosphate glasses for rare-earth-doped ion-exchanged optical waveguide lasers

Sanna Yliniemi

Optoelectronics Laboratory, Helsinki University of Technology, Tietotie 3, P.O. Box 3500, Espoo, FIN-02150 HUT, Finland

Seppo Honkanen

College of Optical Sciences University of Arizona, Meinel Building, 1630 East University Boulevard, Tucson, Arizona 85721

Anatoli Ianoul, Albane Laronche, and Jacques Albert

Department of Electronics, Carleton University, 1125 Colonel By Drive, Ottawa, Ontario, Canada K1S 5B6

Received May 12, 2006; revised August 7, 2006; accepted August 29, 2006; posted August 30, 2006 (Doc. ID 70886)

Phosphate glasses containing enough sodium to allow the fabrication of optical channel waveguides by ion exchange are photosensitive to intense ultraviolet irradiation from excimer lasers at 193 and 248 nm. Permanent submicrometer-period volume index gratings with modulation amplitudes larger than 10^{-4} were obtained even after annealing the irradiated samples for 2 h at 230 °C. Ultraviolet–visible absorption changes were measured in the irradiated areas, as well as structural modifications observed by surface profiling. Comparative studies were carried out for glasses that were also codoped with erbium and ytterbium to provide high gain at wavelengths near 1.5 μm. Finally, we demonstrate narrowband gratings with reflectivities larger than 80% in silver ion-exchanged channel waveguides made in these phosphate glass substrates. © 2006 Optical Society of America

OCIS codes: 050.7330, 130.2790.

1. INTRODUCTION

Phosphate glasses are excellent hosts for erbium with optical gain in the important telecommunication band at approximately 1.55 μm. The main advantages of these glasses over the more commonly used silica and silicate glasses are the high solubility of erbium (and other rare earths) and the weak ion–ion interactions in phosphate glass. These features allow for high concentrations without significant lifetime reduction, thereby leading to much higher gain figures per unit length.[1–6] The typical gain values in such glasses lie between 3–4 dB/cm at optical wavelengths near 1535 nm, and in heavily Er–Yb-codoped phosphate glasses a gain value as high as 4 dB has been measured from only a 3 mm long sample.[6] These highly Er-doped phosphate glasses have allowed the development of compact waveguide and fiber laser sources.[5,7–13] Until recently, the main drawback in using these glasses has been their relative sensitivity to environmental attack and the difficulty in processing them into fibers and waveguide devices. However, phosphate fiber lasers are now being made commercially,[14] and a novel glass (called IOG, from Schott Glass Technologies) has been synthesized especially for the purpose of allowing planar and channel waveguide fabrication by ion exchange.[8] The parameters of this glass were optimized for codoping with rare-earth elements as well as with a significant amount of sodium (Na). The Na^+ ions are weakly bonded to the glass matrix and exchange readily with other ions of the same valence (K^+, Ag^+, and Li^+) when the proper conditions are met (temperature and concentration gradients).[15,16] Using these glasses, it has been possible to demonstrate both waveguide amplifiers[6] and lasers.[5,7–10] In lasers, external reflectors or relief gratings are used to form the laser cavity and to perform wavelength selection out of the broadband gain. It is, however, desirable to use volume holographic gratings as mirrors for the laser cavities for two reasons: (1) relief gratings suffer from large short-wavelength loss bands that prevent the pump light from reaching the cavity through the end reflectors and (2) multilayer thin-film coatings deposited on polished ends represent an expensive process in terms of achieving high reliability in mass production for narrowband operation.

To our knowledge, the first attempts to realize volume Bragg gratings for waveguide mirrors in phosphate glasses were reported only recently, photoinduced index changes in slab waveguides made by silver ion exchange in Er-doped IOG-1 glass were obtained by irradiation with KrF laser light.[17] The estimated refractive index modulation was calculated to be $\sim 2 \times 10^{-3}$ over a depth of 3 μm, a result derived from diffraction measurements of light incident perpendicular to the sample. Furthermore,

it was reported that the index change obtained was 2 orders of magnitude larger in the ion-exchanged region than in the substrate glass alone. This was tentatively attributed to photoinduced silver ion migration and the photoionization of Ag^0 and Ag^+ species. However, the gratings obtained could not be measured or even observed with light guided in these waveguides. We have carried out similar experiments with similar results and have found that the gratings thus obtained were limited to a very thin surface layer and did not overlap enough with guided modes to generate useful reflectivity values. It is the purpose of this paper to propose and study in detail an alternative method for waveguide grating formation (for laser applications) using the photosensitive response of undoped and rare-earth-doped phosphate glasses for laser applications.

In our approach, pulsed excimer laser light (both KrF at 248 nm and ArF at 193 nm) is used to irradiate the substrate glass samples through phase masks to write volume gratings prior to fabricating the waveguides by ion exchange. With this technique, described in Section 2, we have realized Bragg gratings with useful narrowband reflectivities in single-mode channel waveguides. In the remainder of this paper we present the experimental methodologies used to irradiate the glass samples and to measure the photoinduced refractive index changes, absorption changes, and structural modifications. This is followed by the results of the experiments for the various cases and a discussion of their implications in terms of finding the optimum fabrication conditions for waveguide Bragg grating mirrors.

2. EXPERIMENTAL DETAILS

A. Initial Characterization of the Glasses

The IOG-1 glasses used in this work are commercially available.[8] They are composed mostly of P_2O_5 (60 mol. %), with ~24 mol. % of Na_2O to allow waveguide fabrication by ion exchange. The remainder of the glass is made up of Al_2O_3 (~10 mol. %), to improve the chemical durability of the glass, and rare-earth oxides in various combinations (La, Er, Yb, and Nd).[8] For passive glass, labeled as IOG-1 in the following, only lanthanum is used; for the IOG-1-7 active glasses, erbium and ytterbium are added in various ratios to have glasses with gain at approximately 1550 nm (neodymium-doped glasses provide gain near 1064 nm, but they are not studied here). For the waveguide fabrication, we are using the electric-field-assisted silver film ion exchange technique.[18,19] This technique does not involve salt melts or strong etchants and is carried out at a relatively low temperature (90 °C). Therefore this particular form of ion exchange is ideally suited for phosphate glasses that react easily with molten salt baths and with the etchants used to remove conventional diffusion masks, resulting in damage to the surface. It has been shown that a very low propagation loss of 0.15 dB/cm in surface waveguides can be achieved in phosphate active glass by using this technique.[20]

To get permanent refractive index changes from ultraviolet irradiation, some absorption mechanism must be present to trigger the photochemical reaction.[21,22] The ultraviolet absorption characteristics of IOG-1, IOG-1-7, and also of IOG-1 with a 10 μm deep silver ion-exchanged slab waveguide across the whole surface is shown in Fig. 1 [measured with a Cary 500 ultraviolet–visible-near-infrared (UV–Vis–NIR) spectrophotometer]. The transmission results indicate that IOG-1-7 glasses and silver-ion-exchanged glasses are essentially opaque at 193 nm, while the absorption measurements at 248 nm confirm the findings of Ref. 17, i.e., that the penetration depth in the silver ion-exchanged slab IOG-1 is less than 3 μm. On the other hand, IOG-1 is relatively transparent at 248 nm, but there appears to be a wide absorption band (in contrast to a band edge) across shorter UV wavelengths down to at least 193 nm. The low absorption explains the weak photosensitivity of IOG-1 at 248 nm, but we would expect some photosensitivity for IOG-1-7 at that wavelength. The UV–Vis absorption results show clearly that we cannot expect UV-induced gratings to extend fully across the core of typical ion-exchanged waveguides, even more so when such waveguides are buried under the surface to reduce birefringence and improve coupling to optical fibers.

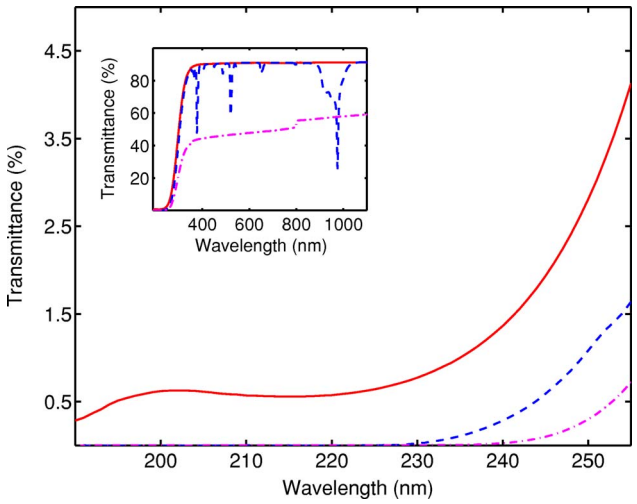

Fig. 1. (Color online) UV–Vis transmission spectra for passive IOG-1 (undoped, red solid curve) and active IOG-1-7 (Er/Yb codoped, blue dashed curve), and for ion-exchanged passive IOG-1 (magenta dash-dotted curve) glass substrates. The thickness of the substrates was 1.5 mm.

B. Irradiation Methodology

A Lumonics PM-848 excimer laser was used to irradiate the samples with high intensity pulses of UV light. The laser was equipped with stable resonator optics for 248 nm operation with a KrF gas mixture, delivering 400 mJ pulses at up to 100 pps. We used a combination of apertures and cylindrical lenses to image a small portion of the excimer output beam onto the sample, with adjustable magnification, and hence power density. The same laser was used at 193 nm with an ArF gas mixture but this time with unstable resonator optics, yielding pulses of 100 mJ. This resonator configuration provided increased spatial coherence, which compensated for the lower gain at 193 nm by allowing tighter focusing of the laser beam output. In most of the experiments described here, the laser ran at 100 pps with an estimated energy density between 140 and 400 mJ/cm^2 per pulse at the

sample (for both wavelengths). One difference is that the pulse length for 248 nm is close to 20 ns, while it is only 14 ns for 193 nm, thereby giving 40% more peak power at the same pulse energy. The irradiations were carried out using different zero-order-nulled phase masks designed to produce submicrometer-period interference patterns immediately behind the mask.[23] Because of the poor spatial coherence of the excimer laser (especially at 248 nm in our case) the mask was placed in close proximity (50–100 μm) to the glass samples to preserve the fringe contrast as deep as possible into the sample.

C. Grating Characterization Techniques

Since no waveguide was present in the glass samples following the grating formation, the grating properties were evaluated by using free-space diffraction of a red He–Ne probe laser beam directed across the sample at various angles of incidence from the sample perpendicular. The diffraction efficiency is defined as the ratio between the power in the transmitted zero-order beam and the various diffracted orders observed.

Further characterization of the irradiated sample was carried out with a stylus profilometer (Tencor P1) and an atomic force microscope (Nanoscope III) for measuring macroscopic and microscopic surface deformations. Finally, the Raman spectra from the irradiated and nonirradiated parts of the sample were measured to determine the effect of UV irradiation on the structural organization in the glass network.

When channel waveguides were fabricated in the samples with gratings (see Subsection 2.D), the grating characteristics were measured by launching broadband light from a pumped Er-doped fiber into the channel waveguides. Light was coupled via butt coupling from a polarization-maintaining single-mode fiber, and the reflected and transmitted light spectra were measured with an optical spectrum analyzer with a 0.01 nm spectral resolution (ANDO AQ6317B). To measure the grating response separately for the two principal polarization states of the channels (quasi-TE and quasi-TM), the light from the broadband source was polarized before being launched into the input fiber.

D. Channel Waveguide Fabrication

The channel waveguides were fabricated in IOG glasses using photoresist masked thin-film silver ion exchange.[19] Mask opening widths ranging from 2 μm to 10 μm were patterned in photoresist with a standard lithography process. The waveguide pattern was aligned visually to lie perpendicular to the grating lines by using the sample edge as a reference. Patterned photoresist was used as a diffusion barrier during the electric-field-assisted ion exchange of silver from a thin silver film sputtered onto the resist coated sample. The ion exchange was performed at 90°C for 2 h with an applied voltage of 200 V. The residual silver film and photoresist were removed, and the sample was annealed at 230°C for 90 min. These conditions led to the formation of approximately 6 μm deep graded index channels that were single mode at wavelengths near 1.5 μm for mask opening widths under 4 μm.

3. EXPERIMENTAL RESULTS

A. Gratinqs in Existing Slab and Channel Waveguides

Our first experiments were aimed at confirming the results reported by Pissadakis *et al.*[17] Gratings were written at 248 nm in slab waveguides made from IOG-1 glass. Strong coloration appeared after 50 pulses, and it saturated after 500 pulses. Following the irradiation, the free-space diffraction of the samples was probed. Two regimes were observed: For irradiations below 50 pulses, the diffraction pattern at normal incidence consisted of multiple orders on either side of the zeroth-order transmitted beam. This indicated a thin surface grating operating in the Raman–Nath regime. For longer irradiations the diffraction efficiency diminished, but when the irradiations exceeded 5000 pulses a new grating appeared that only diffracted a single order at an angle of incidence of 30°. This is an indication of a thick grating operating in the Bragg regime. The maximum diffraction efficiency of the volume grating did not exceed 0.2%. We then proceeded to test ion-exchanged channel waveguides in IOG-1 glasses irradiated at 248 nm. In all cases, a reflection peak with a reflectivity between 1% and 12% appeared with a grating length of 10 mm after a few pulses of irradiation, and the reflectivity did not increase with further pulses. The reflection and transmission spectra measured from the best grating produced in this way are shown in Fig. 2. The grating reflectivity of 12% corresponds to an index modulation of 2×10^{-5}, a value too low for most practical applications. The grating is eventually erased for longer irradiation. We observed that heat was generated during irradiation since the grating wavelength then drifted noticeably and reversibly. We also noted qualitatively that the grating reflectivity grew somewhat stronger when the irradiations were purposely displaced laterally on either side of the channel waveguides, in a region without silver ions.

B. Volume Gratings in IOG-1 Substrates

The latter result in Subsection 3.A is an indication that better gratings are formed in regions of the glass without silver, this time in contrast to what was reported in Ref. 17. To resolve this question, further investigations were carried out in glass samples without waveguides. First, IOG-1 glass was irradiated at 193 nm through a 1065 nm period phase mask, yielding an interference fringe pattern with a periodicity of 532.5 nm. The first observable

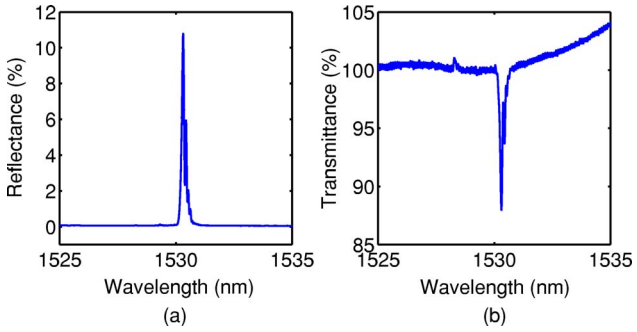

Fig. 2. (Color online) Weak Bragg grating written *in situ* at wavelength 248 nm to the ion-exchanged channel waveguide. (a) Reflectance and (b) transmittance spectrum.

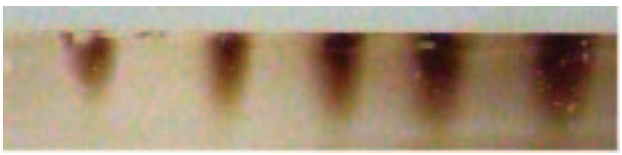

Fig. 3. Coloration caused by the UV exposure. Sample cross sections showing irradiated areas for different exposure times (from left to right): 0.9, 1.8, 3.6, 9, and 18 kJ/cm^2.

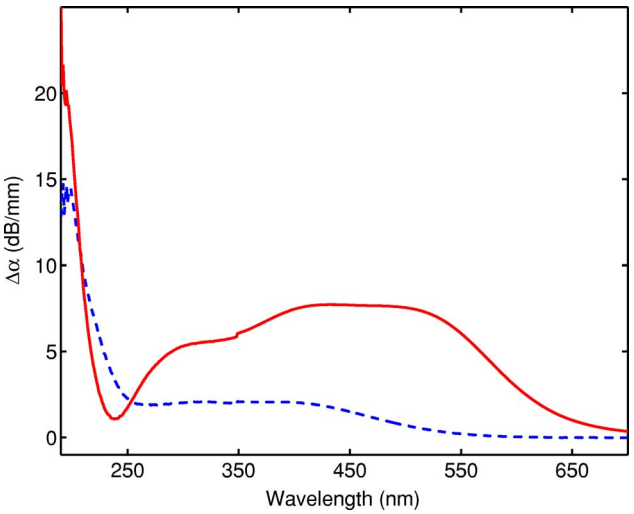

Fig. 4. (Color online) Change in absorbance ($-1/l \log T_i$) due to the UV irradiation and annealing for passive IOG-1 glass. Red solid curve refers to the induced absorbance in the UV-irradiated sample and blue dashed curve to the induced absorbance in the UV-irradiated and annealed sample.

consequence of the irradiation was the appearance of a dark brownish red coloring extending below the surface of the sample. The induced visible coloration strengthened and actually penetrated deeper into the glass for longer irradiations (see Fig. 3 for a picture of the sample cross section showing several irradiated areas for different exposure times). A typical spectrum of induced absorbance is shown in Fig. 4. The absorbance is defined as $-1/l \times \log(T_i)$, where l is the effective penetration depth of the irradiation, and T_i is the internal transmittance. We also note from Fig. 4 that there is a strong increase in absorption at the shortest observable wavelengths, and a broad absorbance peak at approximately 460 nm appears. According to the Kramers–Kroenig relationships, these absorption changes should also give rise to refractive index changes.[24] Since the irradiations were carried out with a sinusoidal interference pattern, the formation of the gratings inside the glass was verified by free-space diffraction. It turns out that no diffraction occurred at normal incidence, but sharp diffracted beams were observed for several values of the angle of incidence. This shows that gratings are formed and that they operate in the Bragg regime (the grating thickness is large relative to the probing wavelength). The strongest diffraction always occurred at an angle of incidence of $36 \pm 1°$ from the surface normal. In the Bragg regime, first-order diffraction occurs when $\sin \theta_B = \lambda_0/(2\Lambda)$, where θ_B is the external angle of incidence, λ_0 is the free-space wavelength of the interrogating beam, and Λ is the grating period. Using 36° for the Bragg angle, we get the period of the written grating to be 535 ± 15 nm, in good agreement with the expected value of 532.5 nm corresponding to one half of the phase mask period. While the gratings were observed for relatively short irradiations, the diffraction reached a maximum and started to diminish for longer irradiation times (several minutes). In such cases, however, some diffraction was observed near the edges of the overexposed areas, a possible indication that the disappearance of diffraction resulted from a saturation of the index change and a loss of fringe contrast. This was confirmed by heat treatment of the samples.

The thermal stability of the exposed gratings must be tested for two main reasons: first, to ensure the long-term reliability of such gratings at normal temperatures, and second, to verify how much grating strength would remain if we were to attempt fabricating waveguides in the samples after the gratings were written. The samples were placed on hot plates at 230 °C for 2 h, and the grating diffraction was remeasured afterward. It turns out that after this annealing step, the gratings that had good diffraction originally had mostly disappeared, while those that were originally overexposed ended up with significant diffractive power. The diffraction efficiency and the height of the surface ridge for gratings written at different irradiation doses are shown in Fig. 5. The surface swelling reached a height of nearly 700 nm for a UV irradiation dose of 60 kJ/cm^2. Assuming an average effective depth of 300 μm for the irradiated glass (see Fig. 3), this corresponds to a density decrease ($\Delta V/V$) of the order of 0.002. Obviously, this is a very rough estimate that does not take into account the restraining effect of the surrounding substrate and many other structural factors. However, this value is not out of line with the estimated refractive index changes obtained from the grating measurements (see Subsection 3.D). The dark brown color observed after the irradiation was also removed significantly by the thermal process, leaving just enough pale yellow color to facilitate locating the grating areas. The partial erasure of the UV-induced absorption can be observed in the absorption measurements of Fig. 4. More specifically, the broad absorbance peak at approximately

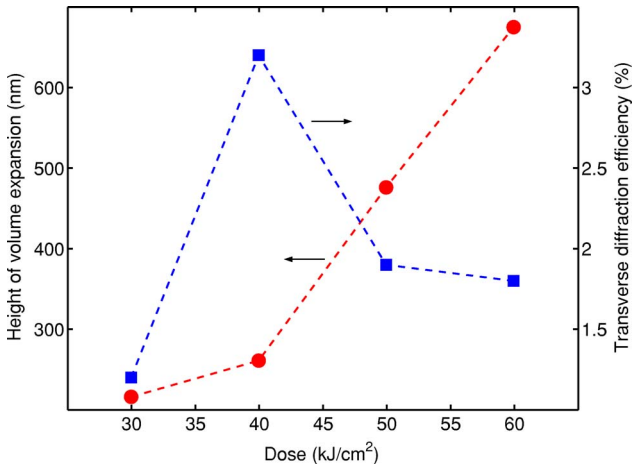

Fig. 5. (Color online) Diffraction efficiency (blue squares) and the height of the surface swelling (red circles) as functions of the UV irradiation dose. The red and blue lines between the markers have been drawn for the eye.

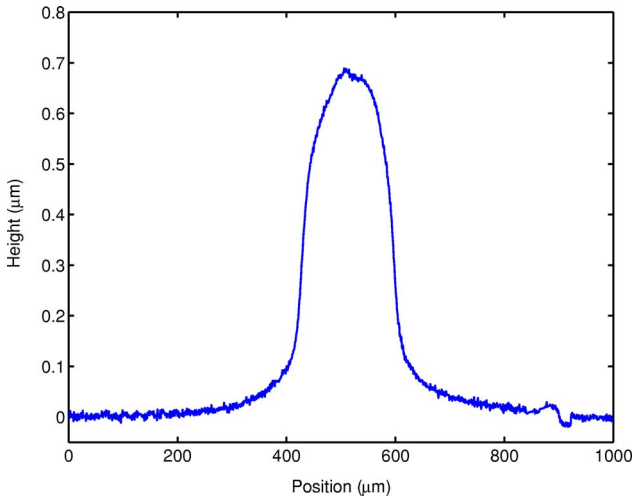

Fig. 6. (Color online) Surface ridge measured by a Tencor P1 profilometer.

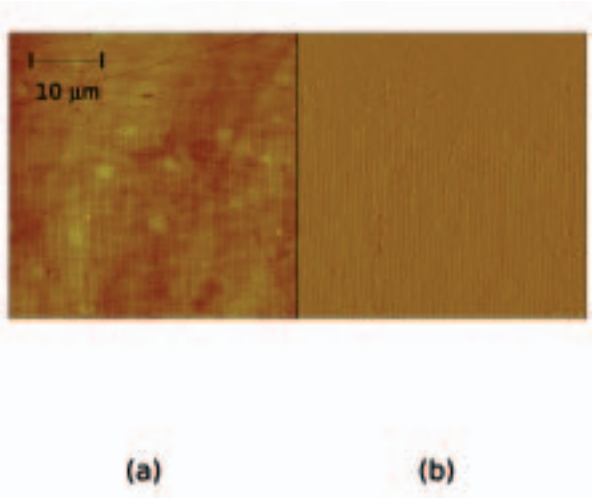

Fig. 7. (a) AFM topography and (b) deflection images of a glass sample exposed to UV irradiation. Topography scale is 35 nm. Atomic force microscopy measurements were carried out on a multimode Nanoscope III atomic force microscope (Digital Instruments, Santa Barbara, Calif.) in the repulsive mode in air. A J scanner (maximal scan area of 120 m2) and 200 m long soft cantilevers with integrated pyramidal silicon nitride tips (spring constant of 60 mN/m) were used. The imaging force was approximately 2–4 nN, and the scan rate was typically 0.5 Hz.

the 460 nm wavelength approaches the original spectrum of the pristine sample after annealing, whereas only a minor recovery toward the original sample absorbance level is observed at shorter wavelengths.

Further information is provided by the surface topography of the irradiated samples. A scan with a stylus-type profilometer revealed that broad surface ridges had formed in the irradiated areas. The result is shown in Fig. 6. Finer scale topographic features can also be observed by using atomic force microscopy: Figure 7 shows that a submicrometer-period surface grating with less than 30 nm of amplitude is superimposed on the 700 nm high ridge. The origin of the observed volume changes may be inferred from an examination of the differences in the Raman spectra of the irradiated and base glasses, shown in Fig. 8. We observed a 10% change in the ratio of the P–O–P (with a bridging oxygen) to the O–P–O (with two terminal oxygens) symmetric modes, indicating that the ArF irradiation had broken some chemical bonds and had rearranged the network structure of the glass.[25,26] An increase in the intensity ratio of $\nu(PO_2)/\nu(POP)$ suggests that depolymerization had taken place, and the phosphate chains in the glass matrix had been shortened. These results are in agreement with the observed surface swelling: Once the glass material becomes more crystalline it will expand in the direction normal to the surface.

To estimate the refractive index modulation amplitude of the fabricated gratings, we need to know their period and the depth of the grating fringes. Theoretically, the diffraction efficiency of the grating, $\eta = I_{\text{diff}}/I_0$, is related to the grating parameters by

$$\eta = \sin^2[2\pi d\Delta n/(\lambda_0 \cos \theta_{Bi})], \tag{1}$$

where d is the thickness of the grating, Δn is the refractive index modulation amplitude of the sinusoidal grating, and θ_{Bi} is the internal angle relative to the sample perpendicular.[27] Again assuming an effective depth of 300 μm at the maximum observed diffraction efficiency of 3%, a lower bound for the amplitude of the index modulation is 1×10^{-4} (or 2×10^{-4} peak-to-peak). Note that with this value of index modulation in a channel waveguide, narrowband reflectivities of 93% are achievable with a grating length of only 1 cm.

C. Volume Gratings in IOC-1-7

Similar experiments were carried out in IOG-1-7 Er–Yb codoped substrates, but at 248 nm since the penetration depth of 193 nm radiation in these glasses would be negligible (from Fig. 1). Figure 9 shows the UV-induced absorption of IOG-1-7 using KrF irradiation, as well as the

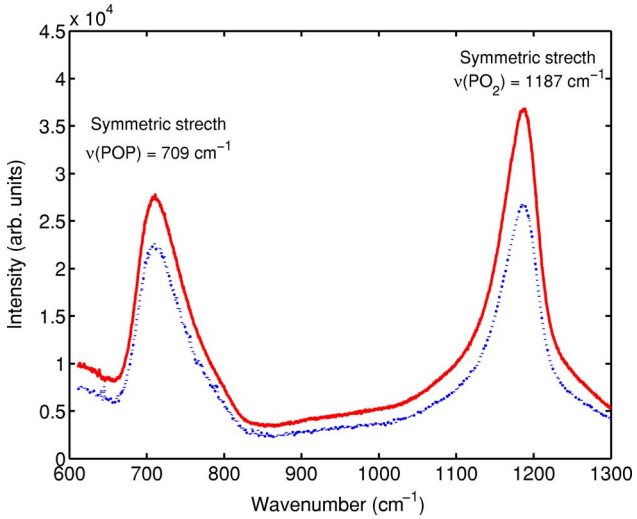

Fig. 8. (Color online) Raman spectra measured for UV-irradiated (red solid curve) and non-UV-irradiated (blue dotted curve) areas of the sample. Raman measurements were performed using a single-grating monochromator (Jobin Yvon, focal length 640 mm) equipped with a liquid-nitrogen-cooled CCD camera (Princeton Instruments) and a notch filter to remove the excitation wavelength. An air-cooled argon ion laser (Melles Griot) operating at 488 nm 100 mW was used as an excitation source. The spectral resolution of the instrument was 4 cm^{-1}. The accumulation time was 60 s.

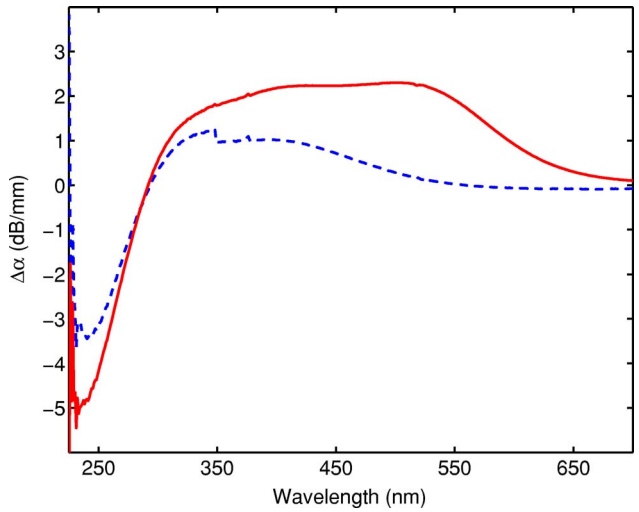

Fig. 9. (Color online) Change in absorbance $(-1/l \log T_i)$ due to the UV irradiation and annealing for active IOG-1-7 glass. Red solid curve refers to the induced absorbance in the UV-irradiated sample, and blue dashed curve to the induced absorbance in the UV-irradiated and annealed sample.

thermal erasure of this coloring. The results are markedly different: The induced absorption at visible wavelengths is significantly smaller, and there is a decrease in absorption, or bleaching, observed near the irradiation wavelength. Annealing the sample recovers the absorption close to the preannealed level. The net integrated absorption changes across the spectrum are therefore much smaller than in the previous case (see Figs. 4 and 9) and would indicate smaller refractive index changes. The best diffraction efficiency achieved in active glass is 0.5% before annealing (and 0.1% after annealing at 230°C for 2 h), an order of magnitude less than in IOG-1 with ArF. The smaller diffraction efficiencies obtained are at least partly due to the reduced fringe contrast for our system at 248 nm (as discussed above), but they also arise from the reduced net absorption changes. Furthermore, we were not able to detect a measurable swelling of the glass surface under KrF irradiation even for long exposure times.

D. High Reflectivity Gratings in Channel Waveguides

Following up on the results of Subsection 3.B, a new sample of IOG-1 was irradiated for 5 min at 100 pps in the same conditions as above to yield an overexposed grating 4 mm in length. A set of channel waveguides was then fabricated in this sample. Following all the waveguide fabrication steps, the UV-induced coloring had almost completely disappeared (to a greater extent than that shown in Fig. 3); but a clear Bragg grating resonance was observed in the waveguide transmission spectrum. Figure 10 shows the measured reflection and transmission spectra of the fabricated waveguide. A −2.5 dB transmission notch occurs near 1608 nm, corresponding to a reflection of 44%, with no evidence of coupling to radiation or cladding modes.[28] This Bragg wavelength corresponds to a grating period of 532.5 nm when the effective index of the waveguide (1.51) is taken into account. The absence of noticeable cladding mode resonances indicates a good overlap of the guided mode with the grating planes and also that the grating planes are quite perpendicular to the waveguide axis in spite of the crude alignment procedure used. If the overlap is close to unity, the measured reflectivity corresponds to an index modulation of 1.0×10^{-4}. Since the coupling coefficient is directly proportional to the product of the overlap and the index modulation, if the overlap is lower, the index modulation is higher by a similar ratio. These results are consistent with the index modulation amplitude evaluated from the free-space diffraction experiments.

Again, similar experiments were carried out with IOG-1-7, but at 248 nm. The samples were irradiated for 30 min at 100 pps using 250 mJ/cm^2/pulse, and single-mode channel waveguides were subsequently fabricated as above. The best channel waveguide reflectivity obtained in these glasses so far was 15% for a 13 mm long uniform grating. This corresponds to a refractive index modulation amplitude of 1.5×10^{-5}. A typical transmission spectrum measured from an active grating with a waveguide is shown in Fig. 11. The transmission notch occurs at a wavelength of 1531.59 nm and corresponds to a transmissivity of 90%.

As a demonstration of the potential of these volume gratings, we have successfully demonstrated laser operation in a hybrid sample of IOG-1/IOG-1-7.[29] A 10 mm long, 80% reflectivity grating was written in the passive section of the substrate by using a phase mask with a period op-

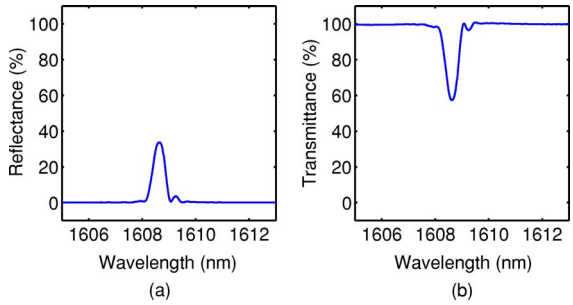

Fig. 10. (Color online) (a) Reflectance and (b) transmittance for a channel waveguide grating in passive IOG-1 glass.

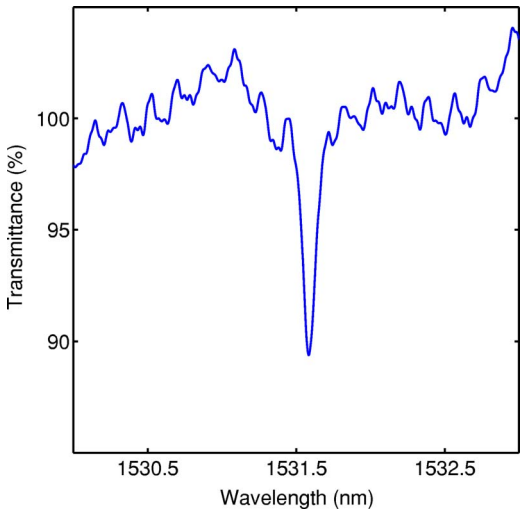

Fig. 11. (Color online) Transmittance for a channel waveguide grating in active IOG-1-7 glass. The ripple around 100% is due to the noise during the measurement.

Table 1. Exposure Parameters

Reflectivity (%)	Length (mm)	Glass	Excimer Laser	Fluence (mJ/cm^2)	Time (min)
12	9	Undoped	KrF	460	4
44	4	Undoped	ArF	300	5
15	13	Er/Yb codoped	KrF	250	30
80	9	Undoped	ArF	140	25

timized for a Bragg reflection near 1535 nm. In this hybrid sample, the gain was provided by a 19 mm long active section fused to the passive substrate. The other mirror of the cavity was provided by a broadband SiO_2/TiO_2 thin-film stack coated directly to the fiber that was also used to deliver the pump power. The laser output power was extracted through the UV-written Bragg grating. For more details, please refer to Ref. 29.

In the channel waveguide gratings in both undoped and Er–Yb-codoped IOG-1, the reflectivity of the gratings showed a 0.2 nm polarization-dependent wavelength shift, corresponding to a waveguide channel birefringence of approximately 2×10^{-4}. No attempt was made to reduce this birefringence, even though the technology to do so exists,[30] because single polarization operation is more desirable for waveguide lasers. We believe that there is room for improvement there as we further optimize the irradiation conditions. Table 1 sets out the parameters (fluence, exposure time, and wavelength) used to fabricate the channel waveguide gratings presented in this paper and in Ref. 29.

4. DISCUSSION

At least two processes contribute to UV-induced refractive index changes in these glasses: (1) the color center redistribution evidenced by absorption changes in the ultraviolet, and (2) the dilatation–densification processes observed in the stylus profilometer and Raman measurements. While the latter processes become very significant for large doses of intense UV light, it is not clear how much they contribute to the required submicrometer-period refractive index modulations. Additionally, it is not clear if structural modifications lead to a decrease or an increase of the refractive index: This depends on the stress redistribution near the sample surface and on the stress–optic coefficient of the glass (see Ref. 31 for example). We attempted to elucidate this by launching light in a sample that was cut and polished perpendicularly to a UV-written line with a 700 nm ridge height, as if this line were a channel waveguide. At the output of the waveguide, some light appeared guided in a crescent-shaped region at the bottom of the UV-exposed area. This seems to indicate that most of this region has experienced a negative index change associated with the dilatation of the glass, except for a small region near the bottom and edges where the substrate network resisted the dilatation by compressing the irradiated glass (as in Ref. 32).

Another point of interest is that relatively strong gratings remained after waveguide formation using a heat treatment even though most of the coloring had disappeared, except in the far UV portion (190–240 nm) of the measured spectrum for IOG-1. This UV-induced absorption near 190 nm in IOG-1 peaked with the noise and could have been attributable either to a band-edge shift associated with the structural modifications or to an absorption band at shorter wavelengths. A spectral signature somewhat similar to that seen here, i.e., the erasure of absorption bands in the UV-Vis spectrum and a remaining band in the vacuum UV region, was observed in ion-implanted silica glasses irradiated with strong excimer laser light pulses.[33] In conclusion, the macroscopic UV-induced structural modifications point to a negative index change, while permanent (heat resistant) color center formation between 190 and 240 nm would contribute positively to the index change. However, the UV-induced index change was too small to be measured by conventional refractive index measurement methods, such as prism coupling. Therefore the origin of the photosensitivity is left as an open question.

The major problem with this type of UV-written grating is the delicate balance that must be maintained between the high fluence needed to access the high index change regimes and the fact that the samples absorb at these wavelengths. The absorption processes generate heat and sometimes catastrophic damage. This requires very good control of the irradiation conditions, and further work is needed to stabilize the process, especially with the active glass samples. It is likely that the improved beam quality arising from the unstable resonator configuration at 193 nm contributes to this control since sample damage was far less a problem in that case. In spite of these problems, we have found reproducible conditions for writing reasonable strength gratings in channel waveguides in both IOG-1 and IOG-1-7 glasses.

5. CONCLUSIONS

We have demonstrated the feasibility of writing high reflectivity, thermally robust, Bragg gratings with excellent spectral characteristics in channel waveguides fabricated in phosphate glasses. This was achieved by irradiating substrate glass samples through a phase mask with high intensity UV light pulses to form a volume hologram inside the glass prior to waveguide fabrication. Passive phosphate glass was observed to be photosensitive for UV irradiation at a wavelength of 193 nm while the active, Er/Yb-codoped, phosphate glass was more sensitive for the UV irradiation at a wavelength of 248 nm (in agreement with Refs. 17 and 22). The refractive index change in passive phosphate glass was shown to be associated with optical absorption changes in the UV and visible spectra, changes in the Raman spectrum, and macroscopic and microscopic structural changes in the glass. It is not possible at this point to determine whether the index change is attributable mainly to color center effects or to structural deformations. It is interesting to note that we did not observe by visual inspection any evidence of surface swelling or volume expansion in the sample of IOG-1 glass that yielded the highest reflectivity grating. Therefore while volume changes do occur in many cases, and most certainly cause average refractive index changes, they are not directly responsible for the observed

refractive index modulations. These NIR refractive index modulations must then be associated either with UV-irradiation induced color center absorption changes through Kramers–Kronig relations or with stress modulation without significant volume change. Thus far, the grating strength achieved in Er–Yb-codoped phosphate glass is significantly weaker than that in the undoped glass, but we are hoping to improve on these results by further studies at 248 nm. The feasibility of making good quality Bragg gratings in phosphate glass channel waveguides is opening up many important applications in compact, narrow-linewidth waveguide laser sources.

ACKNOWLEDGMENTS

This research was supported by the State of Arizona Photonics Initiative (TRIF). S. Yliniemi thanks the Academy of Finland and the Magnus Ehrnrooth Foundation for financial support. This work was performed while S. Yliniemi was with the College of Optical Sciences at the University of Arizona. J. Albert would like to acknowledge the financial support of the Canada Research Chairs Program and the Natural Sciences and Engineering Research Council of Canada.

The e-mail address for S. Yliniemi is sanna.yliniemi@tkk.fi. The e-mail address for J. Albert is jalbert@doe.carleton.ca.

REFERENCES

1. D. Barbier, J. M. Delavaux, A. Kevorkian, P. Gastaldo, and J. M. Jouanno, "Yb/Er integrated optics amplifiers on phosphate glass in single and double pass configurations," in Proceedings of Optical Fiber Communication (Optical Society of America, 1995), paper PD-3.
2. T. Ohtsuki, S. Honkanen, S. I. Najafi, and N. Peyghambarian, "Cooperative upconversion effects on the performance of Er^+-doped phosphate glass waveguide amplifiers," J. Opt. Soc. Am. B **14**, 1838–1845 (1997).
3. Y. C. Yan, A. J. Faber, H. de Waal, P. G. Kik, and A. Polman, "Erbium-doped phosphate glass waveguide on silicon with 4.1 dB/cm gain at 1.535 μm," Appl. Phys. Lett. **71**, 2922–2924 (1997).
4. B. C. Hwang, S. Jiang, T. Luo, J. Watson, S. Honkanen, Y. Hu, F. Smektala, J. Lucas, and N. Peyghambarian, "Erbium-doped phosphate glass fibre amplifiers with gain per unit length of 2.1 dB/cm," Electron. Lett. **35**, 1007–1009 (1999).
5. S. Blaize, L. Bastard, C. Cassagnètes, and J. E. Broquin, "Multiwavelength DFB waveguide laser arrays in Yb-Er codoped phosphate glass phosphate glass substrate," IEEE Photon. Technol. Lett. **15**, 516–518 (2003).
6. F. D. Patel, S. DiCarolis, P. Lum, S. Venkatesh, and J. N. Miller, "A compact high-performance optical waveguide amplifier," IEEE Photon. Technol. Lett. **16**, 2607–2609 (2004).
7. D. L. Veasey, D. S. Funk, N. A. Sanford, and J. S. Hayden, "Arrays of distributed-Bragg-reflector waveguide lasers at 1536 nm in Yb/Er codoped phosphate glass," Appl. Phys. Lett. **74**, 789–791 (1999).
8. D. L. Veasey, D. S. Funk, P. M. Peters, N. A. Sanford, G. E. Obarski, N. Fontaine, M. Young, A. P. Peskin, W.-C. Liu, S. N. Houde-Walter, and J. S. Hayden, "Yb/Eb-codoped and Yb-doped waveguide lasers in phosphate glass," J. Non-Cryst. Solids **263–264**, 369–381 (2000).
9. P. Madasamy, G. Nunzi Conti, P. Pöyhönen, M. M. Morrell, D. F. Geraghty, S. Honkanen, and N. Peyghambarian, "Waveguide distributed Bragg reflector laser arrays in erbium-doped glass made by dry Ag film ion exchange," Opt. Eng. (Bellingham) **41**, 1084–1086 (2002).
10. P. Madasamy, S. Honkanen, D. F. Geraghty, and N. Peyghambarian, "Single-mode tapered waveguide laser in Er-doped glass with multimode diode pumping," Appl. Phys. Lett. **82**, 1332–1334 (2003).
11. T. Qiu, L. Li, A. Schülzgen, V. L. Temyanko, T. Luo, S. Jiang, A. Mafi, J. V. Moloney, and N. Peyghambarian, "Generation of 9.3 W multimode and 4 W single-mode output from 7-cm short fiber lasers," IEEE Photon. Technol. Lett. **16**, 2592–2594 (2004).
12. T. Qiu, S. Suzuki, A. Schülzgen, L. Li, A. Polynkin, V. Temyanko, J. V. Moloney, and N. Peyghambarian, "Generation of watt-level single-longitudinal-mode output from cladding-pumped short fiber lasers," Opt. Lett. **30**, 2748–2750 (2005).
13. L. Li, A. Schülzgen, V. L. Temyanko, T. Qiu, M. M. Morrell, Q. Wang, A. Mafi, J. V. Moloney, and N. Peyghambarian, "Short-length microstuctured phosphate glass fiber lasers with large mode areas," Opt. Lett. **30**, 1141–1143 (2005).
14. http://www.npphotonics.com.
15. A. Tervonen, S. Honkanen, and M. Leppihalme, "Control of ion-exchanged waveguide profiles with Ag thin-film sources," J. Appl. Phys. **62**, 759–763 (1987).
16. A. Tervonen, "A general model for fabrication processes of channel waveguides by ion exchange," J. Appl. Phys. **67**, 2746–2752 (1990).
17. S. Pissadakis, A. Ikiades, P. Hua, A. K. Sheridan, and J. Wilkinson, "Photosensitivity of ion-exchanged Er-doped phosphate glass using 248 nm excimer laser radiation," Opt. Express **12**, 3131–3136 (2004).
18. S. Honkanen, A. Tervonen, H. von Bagh, A. Salin, and M. Leppihalme, "Fabrication of ion-exchanged channel waveguides directly into integrated circuit mask plates," Appl. Phys. Lett. **51**, 296–298 (1987).
19. P. Pöyhönen, S. Honkanen, A. Tervonen, and M. Tahkokorpi, "Planar 1/8 splitter in glass by photoresist masked silver film ion exchange," Electron. Lett. **27**, 1319–1320 (1991).
20. P. Madasamy, "Fabrication and characterization of erbium-doped waveguide amplifiers and lasers," Ph.D. dissertation (University of Arizona, 2003).
21. F. Bilodeau, B. Malo, J. Albert, D. C. Johnson, K. O. Hill, Y. Hibino, M. Abe, and M. Kawachi, "Photosensitization of optical fiber and silica-on-silicon/silica waveguides," Opt. Lett. **18**, 953–955 (1993).
22. B. Malo, J. Albert, F. Bilodeau, T. Kitagawa, D. C. Johnson, K. O. Hill, K. Hattori, Y. Hibino, and S. Gujrathi, "Photosensitivity in phosphorus-doped silica glass and optical waveguides," Appl. Phys. Lett. **65**, 394–396 (1994).
23. K. O. Hill, B. Malo, F. Bilodeau, D. C. Johnson, and J. Albert, "Bragg gratings fabricated in monomode photosensitive optical fiber by UV exposure through a phase mask," Appl. Phys. Lett. **62**, 1035–1037 (1993).
24. D, P. Hand and P. St. J. Russell, "Photoinduced refractive index changes in germanosilicate fibers," Opt. Lett. **15**, 102–104 (1990).
25. J. E. Pemberton, L. Latifzadeh, J. P. Fletcher, and S. H. Risbud, "Raman spectroscopy of calcium phosphate glasses with varying CaO modifier concentrations," Chem. Mater. **3**, 195–200 (1991).
26. G. Le Saoût, P. Simon, F. Fayon, A. Blin, and Y. Vaills, "Raman and infrared study of $(PbO)_x(P_2O_5)_{(1-x)}$ glasses," J. Raman Spectrosc. **33**, 740–746 (2002).
27. A. Yariv, *Optical Electronics in Modern Communications*, 5th ed. (Oxford U. Press, 1997), Chap. 12.
28. J. Albert, S. Yliniemi, S. Honkanen, A. Andreyuk, and A. Steele, "UV-written Bragg gratings in silver ion-exchanged phosphate glass channel waveguides," in *Proceedings of the 2005 Topical Meeting on Bragg Gratings, Photosensitivity and Poling*, B. Eggleton, ed. (Sydney, Australia, 2005), pp. 402–404.
29. S. Yliniemi, J. Albert, Q. Wang, and S. Honkanen, "UV-

exposed Bragg gratings for laser applications in silver-sodium ion-exchanged phosphate glass waveguides," Opt. Express **14**, 2898–2903 (2006).
30. D. F. Geraghty, D. Provenzano, M. M. Morrell, J. Ingenhoff, B. Drapp, S. Honkanen, A. Yariv, and N. Peyghambarian, "Polarisation-independent Bragg gratings in ion-exchanged glass channel waveguides," Electron. Lett. **36**, 531–532 (2000).
31. A. Brandenburg, "Stress in ion-exchanged glass waveguides," J. Lightwave Technol. **LT-4**, 1580–1593 (1986).
32. J. Albert and G. L. Yip, "Stress-induced index change for K^+-Na^+ ion exchange in glass," Electron. Lett. **23**, 737–738 (1987).
33. M. Verhaegen, J. L. Brebner, L. B. Allard, and J. Albert, "Ion implantation-induced strong photosensitivity in high-purity fused silica: correlation of index changes with VUV color centers," Appl. Phys. Lett. **68**, 3084–3086 (1996).